J. Cent. South Univ. (2020) 27: 325−333
DOI: https://doi.org/10.1007/s11771-020-4298-x

Springer

Influence of long-term isothermal aging on microstructure and creep rupture properties of Ni-base superalloy M4706

DUAN Yu-hao(段宇浩)[1], ZHANG Peng(张鹏)[1, 2], LI Jiao(李娇)[3], LI Bo(李波)[1], SONG Xiao-long(宋小龙)[1], GONG Xiu-fang(巩秀芳)[4], YANG Gong-xian(杨功显)[4]

1. State Key Laboratory for Mechanical Behavior of Materials, Xi'an Jiaotong University, Xi'an 710049, China;
2. Xi'an Thermal Power Research Institute Co., Ltd., Xi'an 710032, China;
3. Instrumental Analysis Center, Xi'an Jiaotong University, Xi'an 710049, China;
4. State Key Laboratory for Long-life High Temperature Materials, Dongfang Turbine Co., Ltd., Deyang 618000, China

Abstract: After a standard heat treatment, the microstructural evolution with time during isothermal aging at 850 °C and its effect on the creep rupture properties of the Ni-base superalloy M4706 at 870 °C and 370 MPa are investigated. It is found that as the aging time increases from 0 to 5000 h, the average diameter of coarse γ' increases from 241 to 484 nm, and the distribution of the carbides at grain boundaries changes from discontinuous to continuous. Moreover, experimental observations on the microstructures of all the crept specimens reveal that dislocation bypassing controls the creep deformation. Thus, it is concluded that the transitions in the microstructures result in the degeneration of the creep rupture properties of the experimental alloy with aging time.

Key words: Ni-base superalloy; isothermal aging; microstructure; creep rupture properties

Cite this article as: DUAN Yu-hao, ZHANG Peng, LI Jiao, LI Bo, SONG Xiao-long, GONG Xiu-fang, YANG Gong-xian. Influence of long-term isothermal aging on microstructure and creep rupture properties of Ni-base superalloy M4706 [J]. Journal of Central South University, 2020, 27(2): 325−333. DOI: https://doi.org/10.1007/s11771-020-4298-x.

1 Introduction

Supper alloys with high-temperature properties are indispensable to fabricate aircraft engines or industry gas turbines at high temperature [1, 2]. A novel directionally solidified (DS) Ni-base superalloy M4706 without any Re has been developed in recent years, which owns unique properties and has been considered an applicable material for land-based gas turbine vanes and blades [3]. Tensile and tensile creep experiments on M4706 have proved that this new alloy owns higher tensile strength and creep rupture properties as compared to the directionally solidified Ni-base superalloy GTD-111 [4], DZ 951 [5] and CM247LC [6] at high temperatures, as illustrated in Figure 1.

It is well known that it is coherent that $L1_2$-ordered γ' precipitate (the intermetallic compound Ni_3(Al, Ti, Ta)) renders the enhanced creep-rupture strength of precipitation-hardened

Foundation item: Project(2018BSHQYXMZZ32) supported by the Postdoctoral Science Foundation of Shaanxi Province of China; Project(20192109) supported by the State Key Laboratory for Mechanical Behavior of Materials, China; Projects(2017M623213, 2018M633487) supported by the Postdoctoral Science Foundation of China
Received date: 2019-04-18; **Accepted date:** 2019-08-26
Corresponding author: ZHANG Peng, PhD, Engineer; E-mail: pengzhangnas@163.com; SONG Xiao-long, PhD, Professor; Tel: +86-29-82668695; E-mail: songxl@mail.xjtu.edu.cn; ORCID: 0000-0002-9314-1587

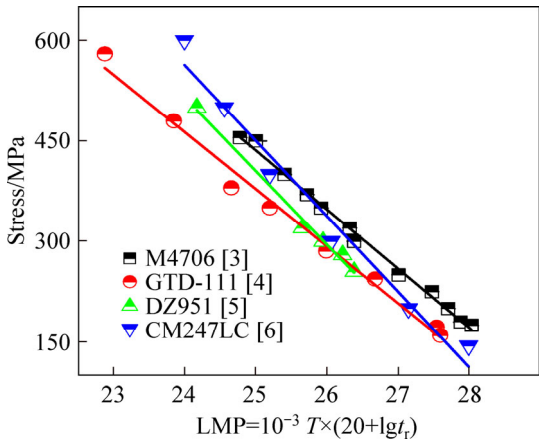

Figure 1 Comparision of Larson-Miller parameter diagram of GTD-111 [4], DZ951 [5], CM247LC [6] and experimental alloy M4706 [3]

Ni-base superalloys [1, 2]. Thus, it is of particular importance for these superalloys to form the γ' precipitates with the optimal size, volume fraction and chemical composition [7−9]. Fortunately, this can be accomplished by changing different chemical composition or altering the heat treatment schedules. Whereas, long-term isothermal aging not only leads to the increase in the particle size of γ' precipitates but also induces the formation of some undesirable topologically close packed (TCP) phases and continuous grain boundary structures, which usually leads to the decrease of mechanical properties of these alloys [9−15]. Therefore, in order to avoid this phenomenon, understanding the relationship among the initial composition, microstructures and associated mechanical properties becomes essential to the alloy designers.

In this work, the impact of isothermal aging on the microstructure and creep rupture properties of M4706 as well as corresponding strengthening/toughening mechanisms is investigated. This investigation has an important effect on understanding the relationship between the initial microstructure and the creep rupture properties.

2 Experimental procedures

The alloy M4706 was a novel DS Ni-base superalloy [16]. Its normal chemical composition is listed in Table 1 for reference. Samples of M4706 with a diameter of around 14 mm were directionally solidified along the [001] direction using an ALD vacuum technologies furnace. Before the creep tests, a standard heat treatment (SHT) was exerted on

Table 1 Nominal chemical compositions of M4706 (wt%)

Co	Cr	W	Ta	Al
9.8−10.3	12.9−13.5	4.3−4.9	4.5−5.1	3.8−4.1
Ti	Mo	C	B	Ni
2.1−2.7	1.5−2.1	0.07	0.013	Bal.

the specimens. The SHT consisted of three steps. Firstly, these specimens were given to a solution heat treatment (1210 °C for 6 h followed by fast air cooling (AC)). Subsequently, the specimens were exposed at 1080 °C for 2 h followed by rapid AC. Finally, the specimens were given an aging heat treatment (850 °C for 24 h, AC). After SHT, the as-heat- treated specimens were aged at 850 °C for up to 5000 h followed by AC.

Threaded specimens were machined from the samples for creep tests. The diameter and gauge length of the specimens were 6.4 mm and 32 mm, respectively. Constant load creep experiments were performed on the specimens after SHT and the specimens after SHT and isothermal aging at 850 °C for different durations using a RD2-3 testing machine at 870 °C for 370 MPa in air (The blades in advanced industry gas turbines usually work at 870 °C). Three R thermal couples were used to control the test temperature and minimize the temperature gradient. During the experiments, the temperature fluctuation was controlled within ±2 °C, and more than two similar specimens were tested for each microstructure.

Microstructures were analyzed using a Zeiss Axiovert 40 MAT optical microscope (OM) and a Zeiss Sigma field emission scanning electron microscope (SEM) equipped with an energy dispersive X-ray (EDX) facility operating at 5 kV. Firstly, specimens for SEM observations were cut from both the thread and gauge section of the failed specimens. Subsequently, the specimens were mechanically ground using silicon carbide papers and polished with 2.5 μm diamond paste. Lastly, the specimens were etched in a solution consisting of 20 mL hydrochloric acid, 20 mL nitric acid, 0.6 g molybdic acid and 30 mL purified water to display the γ matrix and electrolyzed in a solution consisting of 600 mL methyl alcohol and 300 mL phosphoric acid to show the γ' precipitates. The sizes of the γ' precipitates were measured using a line intercept method on the SEM images and the γ'

volume fraction was statistically evaluated according to Ref. [17]. Moreover, transmission electron microscope (JEOL-2100 Plus) operated at 200 kV was used to characterize the deformation microstructures. The specimens were sectioned from cross-sections of the creep samples. After being mechanically lapped to about 50 μm, the TEM foils were prepared by twin-jet electropolishing in a solution consisting of 40 mL $HClO_4$ and 360 mL C_2H_6O at temperatures between −40 °C and −35 °C.

3 Results and discussion

3.1 Microstructural evolution

The typical microstructure of M4706 after SHT is shown in Figure 2(a) and the inset figure. It can be seen that a bimodal distribution of γ' precipitates is obtained for the experimental alloy after this heat treatment. The coarse γ' precipitates appear cuboidal, but the fine γ' precipitates are spheroidal. The SEM images of M4706 after SHT and isothermal aging at 850 °C for 1000, 3000 and 5000 h are separately shown in Figures 2(b)−(d). Clearly, with the increase in the isothermal aging time, the γ' precipitates become larger and larger. The particle sizes of coarse γ' precipitates were measured. The result shows that their average particle sizes are (241±2), (367±3), (454±7) and (484±4) nm, respectively. The γ' volume fractions of the specimens under the four different heat treatments were measured as well. We found that their volume fractions are (49.8±1.1)%, (50.2±1.5)%, (50.0±1.5)% and (50.3±1.1)%, respectively. This result consisted with earlier studies in Refs. [18−22], where as for Ni-base superalloys, the volume fraction of γ' particles is determined only by the isothermal aging temperature, rather than the isothermal aging duration. It is worth mentioning that although after isothermal aging for 5000 h at 850 °C, few TCP phases are visible. This indicates that the isothermal stability of M4706 is excellent.

As stated before, the creep rupture properties of Ni-base superalloy are associated with the carbides, especially those at grain boundaries (GBs) [10, 11]. Thus, the carbides within M4706 are also investigated. As shown in Figure 3(a), considerable amounts of carbides can be observed in M4706 after SHT. Most of these carbides exhibit a blocky morphology. Through the EDX on SEM, it is found that these carbides are rich in C, Ti and Ta and W,

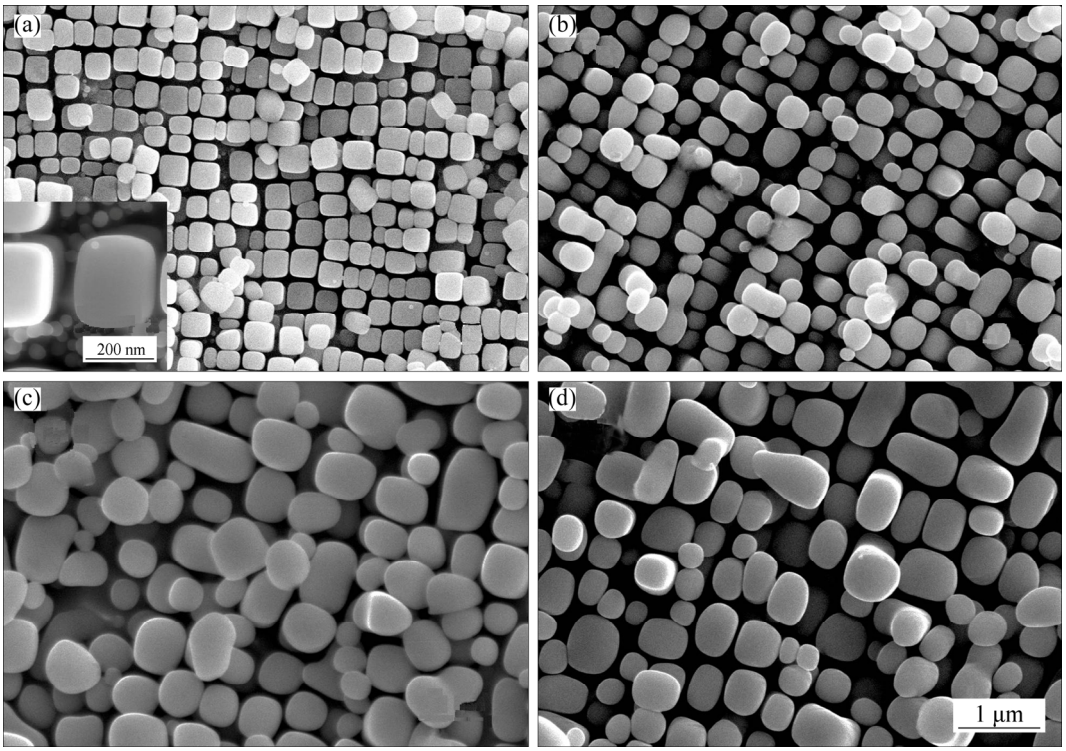

Figure 2 SEM images showing microstructure of M4706 after SHT and isothermal aging at 850 °C for different durations: (a) 0 h; (b) 1000 h; (c) 3000 h; (d) 5000 h (The inset figure in (a) shows fine, spherical γ' precipitates within the matrix)

suggesting that they are MC carbides [1, 10, 11]. After isothermal aging for 1000, 3000 and 5000 h at 850 °C, carbides were also observed in the specimens. Detailed analysis of the microstructures reveals that besides MC carbides, some carbides have a smaller size compared to MC carbides precipitate, and mainly distribute at GBs, as shown in Figures 3(c)−(d). Moreover, from these figures, one can also find that more and more carbides precipitate at GBs so that more and more continuous grain boundary structures (indicated by the white arrowheads) form within the specimens with increasing aging durations. As shown in Figure 4(a), in order to show these structures more clearly, a higher magnification is obtained. Meanwhile, these structures were also observed using SEM. Part of the continuous grain boundary structures formed within the specimens is shown in Figure 4(b). The chemical compositions of the carbides labeled "1", "2", "3" and "4" were also measured. We found that the carbide labeled "1" is rich in Ti and Ta elements, as illustrated in Figure 4(c). Thus, the carbide should be MC carbide. Whereas, the carbides labeled "2", "3" and "4" are rich in Cr element, as illustrated in Figure 4(d). Then, the carbide should be $M_{23}C_6$ [1, 10, 23]. Close inspection of these carbides also reveals that the $M_{23}C_6$ carbides at GBs are usually connected with the MC carbide, as shown in Figure 4(b) and the inset figure. Such a microstructure feature has also been observed in Refs. [10, 23, 24], which suggests that the $M_{23}C_6$ is the product of the decomposition of MC carbide during isothermal aging at 850 °C. Various mechanisms for the transform from MC carbide to $M_{23}C_6$ carbide have been proposed in Ref. [10, 23, 24]. Whereas, considering the fact that the MC carbides are usually surrounded by the $M_{23}C_6$ carbide as well as pores which might be γ' precipitates that are etched out during preparing the specimens in this study, it is tempting to conclude that the formation of $M_{23}C_6$ carbide is via following reaction [10, 23]:

$$MC+\gamma \rightarrow M_{23}C_6+\gamma' \quad (1)$$

Figure 5 reveals the creep rupture properties of M4706 after various heat treatments at 870 °C and 370 MPa. One can see that with increasing aging time, the stress rupture life decreases, namely the longer the aging time, the shorter the stress rupture life. It is worth mentioning that the stress rupture life decreases dramatically after isothermal aging for 1000 h, while the reduction in the stress rupture life decreases slowly as the aging time increases further. This phenomenon might be associated with the changes in the microstructures. This will be

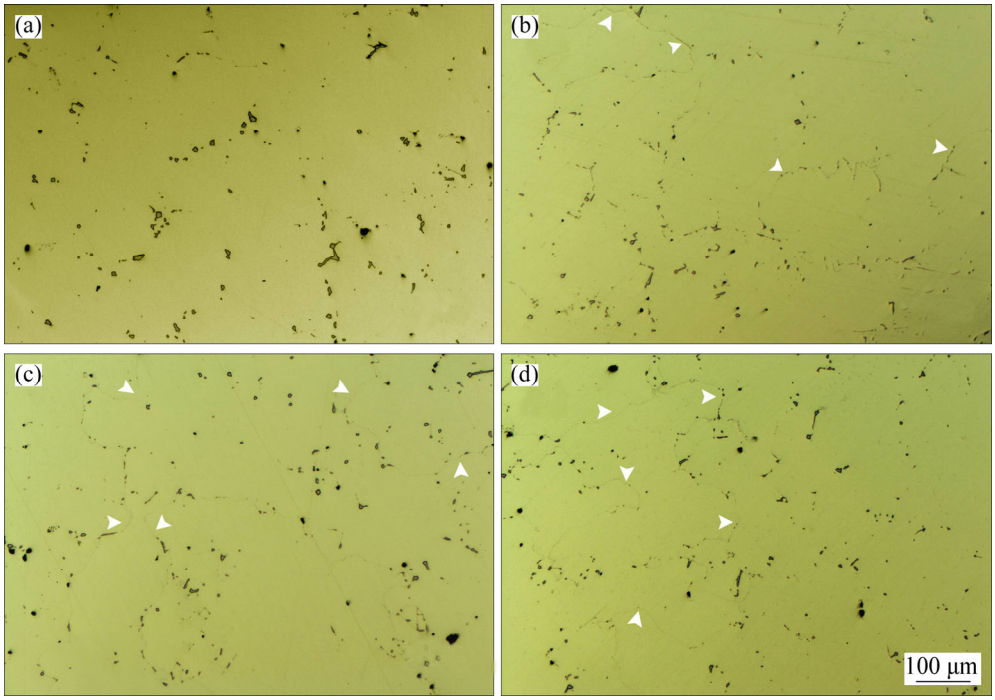

Figure 3 Distribution of carbides at grain boundaries of M4706 after SHT and isothermal aging at 850 °C for different durations: (a) 0 h; (b) 1000 h; (c) 3000 h; (d) 5000 h (The white arrowheads indicate the continuous structures formed by carbides)

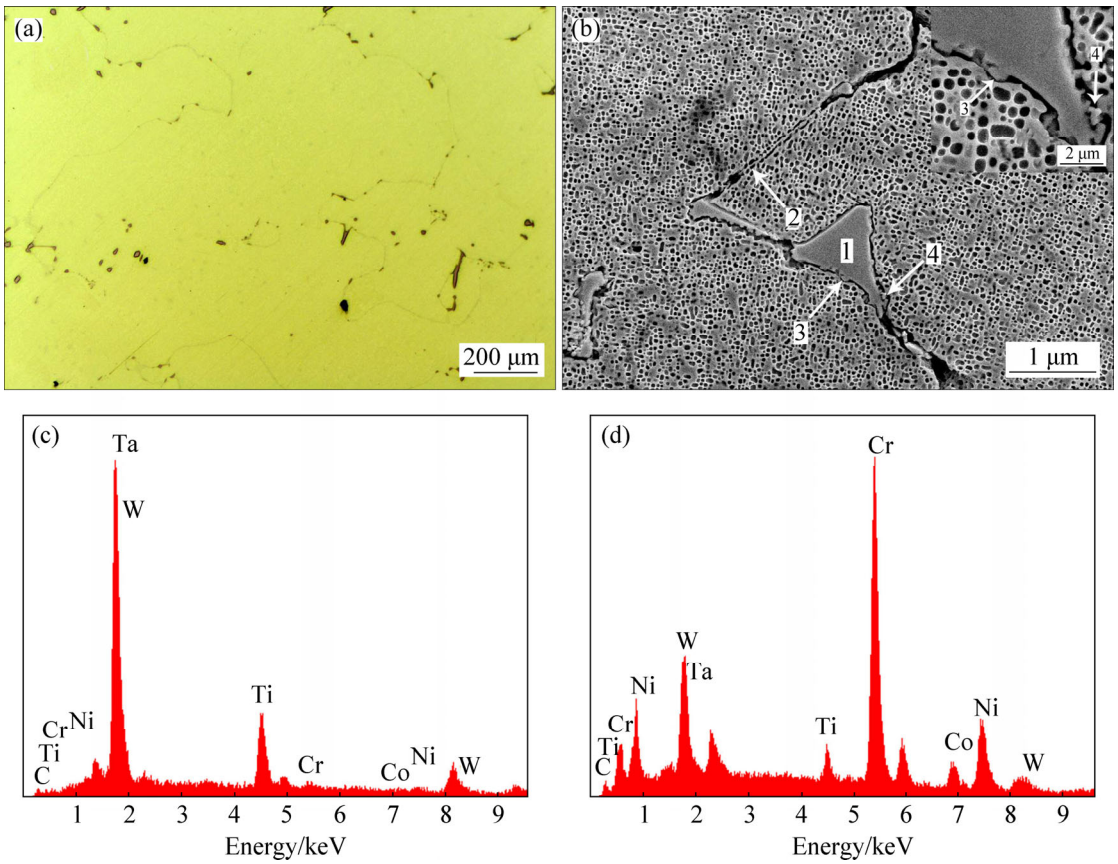

Figure 4 Optical image showing distribution of carbides at grain boundaries, after SHT and 850 °C for 5000 h (a), SEM image showing distribution of carbides at grain boundaries after SHT and 850 °C for 3000 h, inset figure showing the carbides which are connected with the carbide labeled "1" (b), EDS map showing the carbide labeled "1" (c) and EDS map showing the carbide labeled "4" (d)

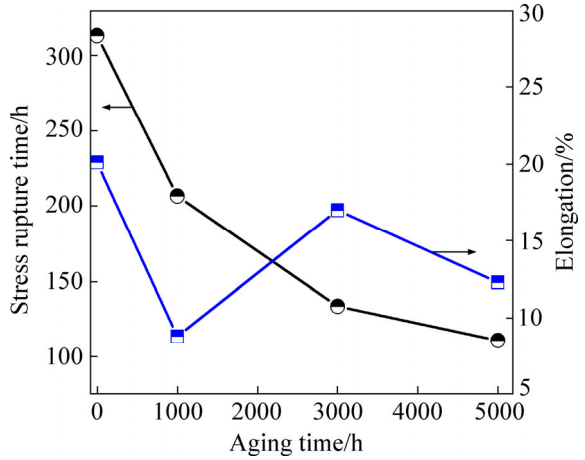

Figure 5 Effect of isothermal aging at 850 °C on creep rupture properties of M4706 tested at 870 °C with an engineering stress of 370 MPa

discussed in Section 3.4. With regard to the elongation to fracture, small fluctuations are observed. Nevertheless, the elongation to fracture for all specimens is above 8.5%, suggesting that M4706 possesses good creep-rupture ductility.

3.2 Deformed microstructures

Figure 6 shows the typical dislocation microstructures of M4706 after different heat treatments and creep deformation at 870 °C and 370 MPa. Although the initial particle sizes of γ' precipitates are not the same, all specimens show similar deformation substructures. After creep deformation, there are few dislocations within the γ' precipitates. However, we can observe many individual bowed dislocations and zigzag dislocations within the γ channel, as shown in Figures 6(a)−(d). Most of these dislocations lie at the γ/γ' interface and the directions of theses dislocations are parallel to the cube edges of γ' precipitates, suggesting that the creep deformation is mainly accomplished by dislocation climb [25, 26]. Further observations of the deformed specimens reveal that many dislocations tangled each other to form the dislocation network, which has been marked up with the white triangles in Figures 6(a)−(d). These deformation patterns

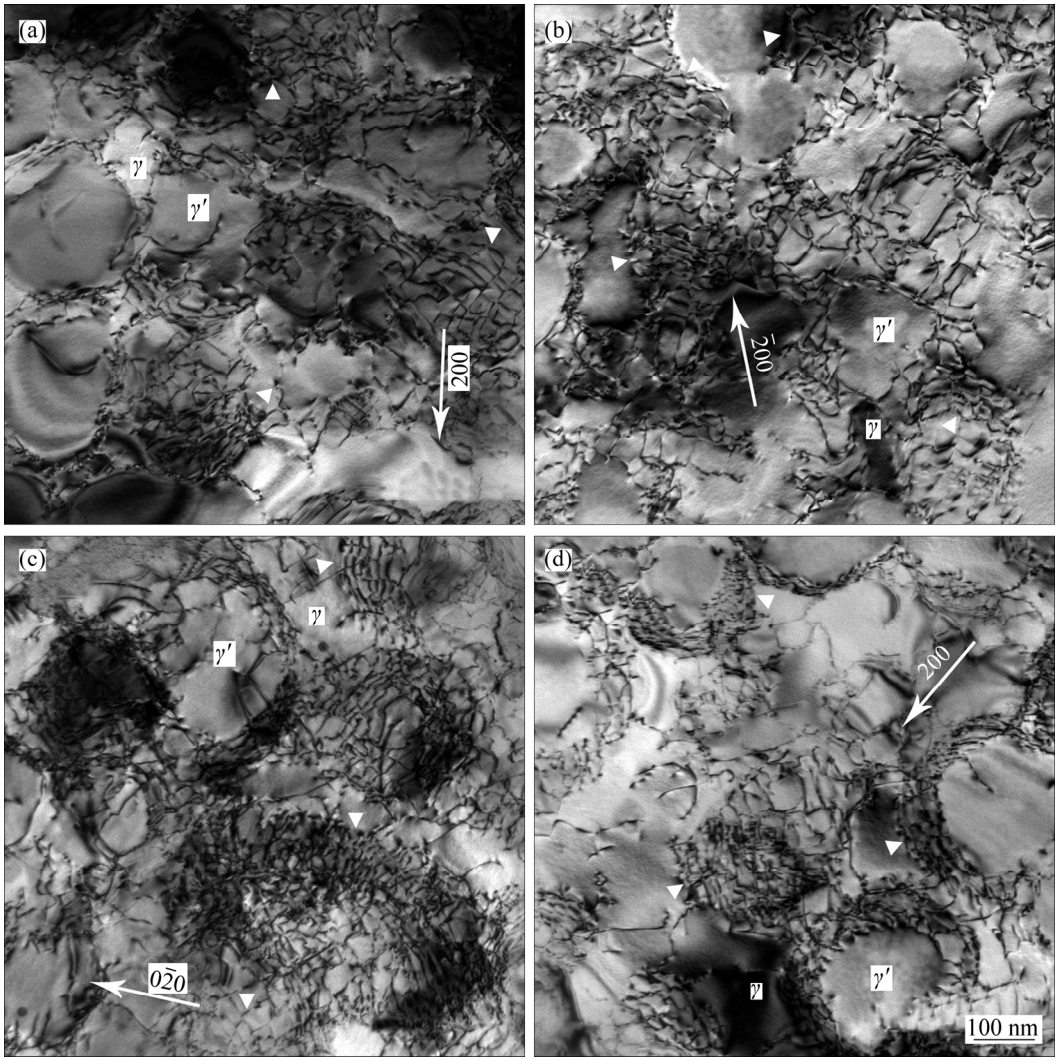

Figure 6 Dislocation structure of M4706 after fracture at 870 °C and 370 MPa: (a) SHT; (b) SHT+(850 °C, 1000 h); (c) SHT+ (850 °C, 3000 h); (d) SHT+ (850 °C, 5000 h) (The white triangles indicate the dislocation networks)

indicate that the γ/γ' interface can strongly impede the movement of matrix dislocation, similar to previous results reported in Refs. [25, 27, 28].

3.3 Correlation between microstructure and creep rupture properties

Now that the dominant deformation mechanism is similar, why the creep rupture life of M4706 shortens with the increasing aging time? In fact, considering the changes in the microstructures, this can be easily explained as below. For DS Ni-base superalloys, most of the creep life is spent on the steady-state creep [5, 11, 29]. Therefore, the steady-state creep rate $\dot{\varepsilon}_m$ usually determines the creep rupture life, which can be represented by the formula [29]:

$$\dot{\varepsilon}_m = A(\sigma - \sigma_p)^n \exp(-Q/(kT)) \tag{2}$$

where T is temperature; σ is the applied stress; Q is the activation energy; A is a constant; σ_p is friction stress; k is the Boltzmann constant; n is a constant stress exponent. During creep deformation, if the applied stress is higher than the Orowan stress σ_o, σ_p is usually set equal to the Orowan stress. Whereas, when the former is lower than the Orowan stress, σ_p is usually set equal to the stress needed for dislocations to climb over the strengthening particle σ_c [29]. According to previous researches [29, 30], σ_o and σ_c can be separately calculated using the following equations:

$$\sigma_o = M \frac{0.81Gb}{2\pi L_s \sqrt{1-\nu}} \ln\left(\frac{d}{2r_i}\right) \tag{3}$$

$$\sigma_c = MR_c \frac{Gb}{2L} \tag{4}$$

$$L = \left(8/3\pi f\right)^{1/2} d \tag{5}$$

$$L_S = 1.235L - d \quad (6)$$

where b is the Burgers vector; M is the Taylor factor; R_c is an unified parameter; G is the shear modulus; d is the mean planar diameter of γ' precipitates; r_i is the inner cut-off distance that is the dislocation core radius with values between b and $4b$; L is the mean planar center-to-center spacing of the γ' precipitates; v is the Poisson ratio and L_s is the surface-to-surface distance between precipitates. Taking Eqs. (3), (5) and (6) or Eqs. (4) and (5) into Eq. (2), one can easily obtain that when the applied stress keeps constant, the steady-state creep rate would increase with increasing the surface-to-surface distance between precipitates. As shown in Figure 2(a), after SHT, fine spherical γ' precipitates in the matrix channel of the experimental alloy. These precipitates can prevent the motion of dislocations within the matrix channel and therefore result in a low creep rate and long-rupture life. However, after long-term isothermal aging at 850 °C, these spherical γ' dissolves and the average size of coarse γ' increases from 241 to 484 nm. As the particle size increases, the surface-to-surface distance between precipitates enlarges as well, since the γ' volume fraction remains unchanged (see Eqs. (5) and (6)). Thus, the stress needed for dislocation to bypass the γ' precipitate via Orowan process or climb decreases significantly during creep deformation. As a consequent, the creep-rupture life shortens significantly after isothermal aging for 1000 h, and the longer the aging time, the shorter the creep rupture life.

On the other hand, from Figure 7(a), we can see that for specimens only subjected to SHT and creep deformation at 870 °C and 370 MPa, most of the carbides still distribute discontinuously at grain boundaries, and creep cracks are rarely visible at these sites after creep deformation. In contrast, after SHT and 850 °C for 5000 h, continuous distribution of carbides formed at grain boundaries and many creep cracks started at the interfaces between grain boundaries and carbides after creep deformation, as indicated by the arrowheads in Figure 7(b). This is consistent with the reported result that the continuous grain boundary structures can promote the initiation and propagation of creep cracks, which usually causes the premature fracture of the specimens [10, 11]. As mentioned above, more and more carbides distribute continuously at grain boundaries within the experimental alloy with the increase in the isothermal durations. Therefore, as the aging time increases, a shorter creep rupture life and lower creep-rupture ductility can be expected.

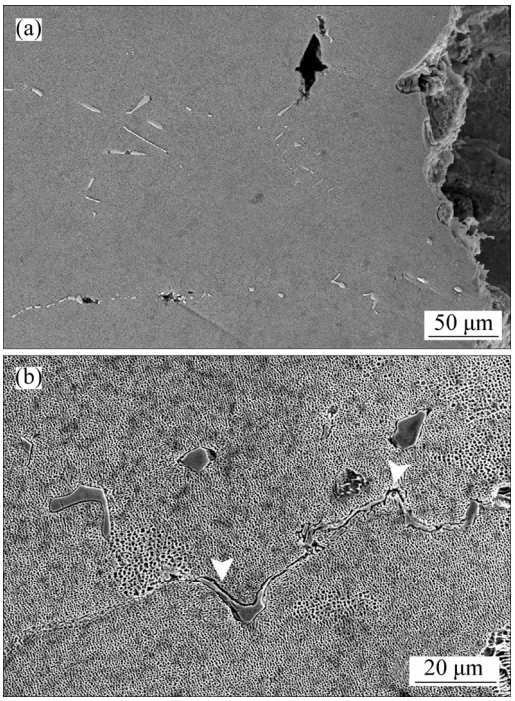

Figure 7 Microstructural changes occurring at grain boundaries of specimens after creep deformation at 870 °C and 370 MPa: (a) SHT; (b) SHT+(850 °C, 5000 h) (The arrowheads indicate the cracks between carbides and matrix)

4 Conclusions

1) After isothermal aging for 5000 h at 850 °C, the average size of coarse γ' precipitates increases from 241 to 484 nm and the γ' volume fraction remains unchanged, suggesting that the experimental alloy possesses excellent microstructural stability.

2) Many $M_{23}C_6$ carbides precipitate at GBs during isothermal aging so that the distribution of carbides at GBs changes from discontinuous to continuous with increasing time.

3) As the aging time increases, the creep rupture life of M4706 at 870 °C and 370 MPa decreases, which is due to the coarsening of γ' precipitates and the formation of continuous distribution of carbides at GBs.

References

[1] REED R C. The superalloys fundamentals and applications

[M]. New York: Cambridge University Press, 2006.

[2] POLOCK T M. Alloy design for aircraft engines [J]. Nature Materials, 2016, 15(8): 809−815. DOI: 10.1038/nmat4709.

[3] ZHANG P, YUAN Y, SHEN S C, LI B, ZHU R H, YANG G X, SONG X L. Tensile deformation mechanisms at various temperatures in a new directionally solidified Ni-base superalloy [J]. Journal of Alloys and Compounds, 2017, 694: 502−509. DOI: 10.1016/j.jallcom.2016.09.303.

[4] SAJJADI S A, NATEGH S, GUTHRIE R I. Study of microstructure and mechanical properties of high performance Ni-base superalloy GTD-111 [J]. Materials Science and Engineering A, 2002, 325(1): 484−489. DOI: 10.1016/S0921-5093(01)01709-9.

[5] CHU Zhao-kuang, YU Jin-jiang, SUN Xiao-feng, GUAN Heng-rong, HU Zhuang-qi. High-temperature creep deformation and fracture behavior of a directionally solidified Ni-base superalloy DZ951 [J]. Metallurgical and Materials Transactions A, 2009, 40(12): 2927−2937. DOI: 10.1007/s11661-009-0001-4.

[6] HASHIZUME R, YOSHIARI A, KIYONO T, MURATA Y, MORINAGA M. Development of novel Ni-based single crystal superalloys for power-generation gas turbines [J]. Materials at High Temperatures, 2007, 24(3): 163−172. DOI: 10.1179/096034007X298516.

[7] VAN SLUYTMAN J S, POLLOCK T M. Optimal precipitate shapes in nickel-base γ-γ' alloys [J]. Acta Materialia, 2012, 60(4): 1771−1783. DOI: 10.1016/j.actamat.2011.12.008.

[8] TIAN Su-gui, TIAN Ning, YU Hui-chen, MENG Xian-lin, LI Ying. Influence of solution temperature on microstructure and creep property of a directional solidified nickel-based superalloy at intermediate temperatures [J]. Materials Science and Engineering A, 2014, 615(7): 469−480. DOI: 10.1016/j.msea.2014.07.103.

[9] LIU J L, JIN T, YU J J, SUN X F, GUAN H, HU Z. Effect of thermal exposure on stress rupture properties of a Re bearing Ni base single crystal superalloy [J]. Materials Science and Engineering A, 2010, 527(4): 890−897. DOI: 10.1016/j.msea.2009.10.001.

[10] QIN X Z, GUO J T, YUAN C, CHEN C L, YE H Q. Effects of long-term thermal exposure on the microstructure and properties of a cast Ni-base superalloy [J]. Metallurgical and Materials Transactions A, 2007, 38(12): 3014−3022. DOI: 10.1007/s11661-007-9381-5.

[11] JIANG X W, WANG D, XIE G, LI H, LOU L H, ZHANG J. The effect of long-term thermal exposure on the microstructure and stress rupture property of a directionally solidified ni-based superalloy [J]. Metallurgical and Materials Transactions A, 2014, 45(13): 6016−6026. DOI: 10.1007/s11661-014-2559-8.

[12] ZHANG P, YUAN Y, LI J, XU Y F, SONG X L, YANG G X. Tensile deformation mechanisms in a new directionally solidified Ni-base superalloy containing coarse γ' precipitates at 650 °C [J]. Materials Science and Engineering A, 2017, 702: 343−349. DOI: 10.1016/j.msea.2017.07.025.

[13] YUAN X F, SONG J X, ZHENG Y R, HUANG Q, YAGI K, XIAO C B, FENG Q. Quantitative microstructural evolution and corresponding stress rupture property of K465 superalloy [J]. Materials Science and Engineering A, 2016, 651: 734−744. DOI: 10.1016/j.msea.2015.11.026.

[14] YUAN X F, SONG J X, ZHENG Y R, HUANG Q, YAGI K, XIAO C B, FENG Q. Abnormal stress rupture property in K465 superalloy caused by microstructural degradation at 975 °C/225 MPa [J]. Journal of Alloys and Compounds, 2016, 662: 583−592. DOI: 10.1016/j.jallcom.2015.12.086.

[15] WU J, LI C, LIU Y C, WU Y, GUO Q, LI H, WANG H. Effect of annealing treatment on microstructure evolution and creep behavior of a multiphase Ni_3Al-based superalloy [J]. Materials Science and Engineering A, 2019, 743: 623−635. DOI: 10.1016/j.msea.2018.11.126.

[16] ZHANG P, YUAN Y, LI B, GUO S W, YANG G X, SONG X L. Tensile deformation behavior of a new Ni-base superalloy at room temperature [J]. Materials Science and Engineering A, 2016, 655: 152−159. DOI: 10.1016/j.msea.2015.12.089.

[17] KOZAR R W, SUZUKI A, MILLIGAN W W, SCHIRRA J J, SAVAGE M F, POLLOCK T M. Strengthening mechanisms in polycrystalline multimodal nickel-base superalloys [J]. Metallurgical and Materials Transactions A, 2009, 40A(7): 1588−1603. DOI: 10.1007/s11661-009-9858-5.

[18] MARTENS V, NEMBACH E. Strengthening of Nimonic alloy PE 16 by ordered particles of Ni_3(Al, Ti) [J]. Acta Metallurgica, 1975, 23(2): 149−153. DOI: 10.1016/0001-6160(75)90178-9.

[19] HEILMAIER M, LEETZ U, REPPICH B. Order strengthening in the cast nickel-based superalloy IN 100 at room temperature [J]. Materials Science and Engineering A, 2001, 319: 375−378. DOI: 10.1016/S0921-5093(01)00989-3.

[20] ZHANG P, YUAN Y, YAN J B, WANG J C, SONG X L, YANG G X. Morphological evolution of γ' precipitates in superalloy M4706 during thermal aging [J]. Materials Letters, 2018, 211: 107−109. DOI: 10.1016/j.matlet.2017.09.096.

[21] WU Yu-ting, LIU Yong-chang, LI Chong, XIA Xing-chuan, WU Jing, LI Hui-jun. Coarsening behavior of γ' precipitates in the γ'+γ area of a Ni_3Al-based alloy [J]. Journal of Alloys and Compounds, 2019, 771: 526−533. DOI: 10.1016/j.jallcom.2018.08.265.

[22] LIU T, WANG J S, DONG J S, WANG L, LOU L H. Effect of heat treatment on microstructure and stress rupture properties of a Ni-Mo-Cr-Fe base corrosion-resistant superalloy [J]. Acta Metallurgical Sinica (English Letters), 2019, 32(1): 116−126. DOI: 10.1007/s40195-018-0837-y.

[23] LVOV G, LEVIT V I, KAUFMAN M J. Mechanism of primary MC carbide decomposition in Ni-base superalloys [J]. Metallurgical and Materials Transactions A, 2004, 35(6): 1669−1679. DOI: 10.1007/s11661-004-0076-x.

[24] WANG J, ZHOU L, SHENG L, GUO J. The microstructure evolution and its effect on the mechanical properties of a hot-corrosion resistant Ni-based superalloy during long-term thermal exposure [J]. Materials and Design, 2012, 39: 55−62. DOI: 10.1016/j.matdes.2012.02.020.

[25] POLLOCK T M, FIELD R D. Dislocations and high-temperature plastic deformation of superalloy single crystals [J]. Dislocations in Solids, 2002, 11: 566−568. DOI: 10.1016/s1572-4859(02)80014-6.

[26] CUI Lu-qing, SU Hu-hu, YU Jin-jiang, LIU Jin-lai, JIN Tao, SUN Xiao-feng. The creep deformation and fracture behaviors of nickel-base superalloy M951G at 900 °C [J]. Material Science and Engineering A, 2017, 707: 383−391.

DOI: 10.1016/j.msea.2017.09.066.
[27] NABARRO F R N, VILLIERS H L D. The physics of creep [M]. London: Taylor and Francis Press, 1996.
[28] TIAN Su-gui, ZHANG Bao-shuai, YU Hui-chen, TIAN Ning, LI Qiu-yang. Microstructure evolution and creep behaviors of a directionally solidified nickel-base alloy under long-life service condition [J]. Materials Science and Engineering A, 2016, 673: 391−399. DOI: 10.1016/j.msea.2016.07.041.
[29] BLUM W, REPPICH B. Creep behaviour of crystalline solids [M]. Swansea: Pineridge Press, 1985: 83−135.
[30] ARDELL A J. Intermetallics compounds as precipitates and dispersoids in high-strength alloys [M]. 1995: 257−286.

(Edited by YANG Hua)

中文导读

长期等温时效对镍基高温合金 M4706 组织和持久蠕变性能的影响

摘要：研究了标准热处理态 M4706 合金在 850 °C 等温时效过程中微观组织结构的演变及其对合金在 870 °C/370 MPa 条件下持久蠕变性能的影响。试验发现，当时效时间从 0 h 增加到 5000 h 时，γ'相的平均尺寸从 241 nm 增加到 484 nm，并且晶界处的碳化物由不连续分布变为连续分布。同时，采用透射电子显微镜对蠕变后的样品进行了观察和分析。试验结果表明，所有热处理态合金的蠕变变形主要是通过基体位错绕过 γ'相来实现的。基于这些结果，认为随着时效时间的延长，这些微观组织结构的变化导致了试验合金的持久蠕变强度随时效时间的延长而不断的恶化。

关键词：镍基高温合金；等温时效；微观组织结构；持久蠕变性能